

# Simultaneous detection of boosted dark matter and neutrinos from the semi-annihilation at DUNE

Mayumi Aoki<sup>1\*</sup> and Takashi Toma<sup>1,2†</sup>

<sup>1</sup>*Institute for Theoretical Physics, Kanazawa University, Kanazawa 920-1192, Japan*

<sup>2</sup>*Institute of Liberal Arts and Science, Kanazawa University, Kanazawa 920-1192, Japan*

## Abstract

Dark matter direct detection experiments impose the strong bounds on thermal dark matter scenarios. The bound can naturally be evaded if the cross section is momentum transfer dependent or velocity dependent. One can test such thermal dark matter scenarios if dark matter particles are boosted by some mechanism. In this work, we consider a specific semi-annihilation  $\chi\chi \rightarrow \nu\bar{\chi}$  where  $\chi$  ( $\bar{\chi}$ ) is dark matter (anti-dark matter), and search for simultaneous detection of the neutrino and the boosted dark matter in the final state at DUNE. We find that the energies of the neutrino and boosted dark matter are reconstructed well due to the precise angular resolution of the DUNE detector. In addition, we find that both signals can be testable at DUNE if the dark matter mass is below 30 GeV, and the scattering cross section is momentum transfer dependent.

---

\*mayumi.aoki@staff.kanazawa-u.ac.jp

†toma@staff.kanazawa-u.ac.jp

# 1 Introduction

Dark matter existing in our universe is being searched by various ways. In particular, direct detection experiments exploring dark matter scatterings with various nuclei such as xenon, argon, germanium etc, have high sensitivities. However no dark matter signal is found so far, and the resultant bounds on dark matter–nucleon scattering cross sections are extremely strong [1–3]. Thus these experiments are starting to rule out thermal dark matter scenarios, which are one of primary dark matter candidates. If one still considers thermal dark matter scenarios, some mechanism is required to suppress scatterings between dark matter and nucleons such as the pseudo-Nambu-Goldstone dark matter [4] and pseudo-scalar interacting fermionic dark matter [5]. In these scenarios, the scattering amplitude is suppressed by a small momentum transfer (or dark matter velocity) while annihilations into normal matter particles are not suppressed. Thus one can obtain the canonical magnitude of the annihilation cross section  $\sim 10^{-26}$  cm<sup>3</sup>/s for thermal dark matter abundance. However it conversely implies that exploring these kinds of models via usual direct detection experiments is extremely difficult.

We still have chance to explore these kinds of models if the dark matter particles are boosted by some mechanism such as scatterings with high energy cosmic-rays [5], vacuum decay [6], heavier dark matter annihilations into lighter ones in multi-component dark matter models [7–16] and semi-annihilations [17–20]. Since the interaction of thermal dark matter itself does not have to be very small to avoid the strong bound of the direct detection experiments, one can search the boosted dark matter at large volume neutrino detectors such as IceCube/DeepCore [21], Super-Kamiokande [22], Hyper-Kamiokande [23] and Deep Underground Neutrino Experiment (DUNE) [24].

In this work, we consider the boosted dark matter produced by the semi-annihilation process  $\chi\chi \rightarrow \nu\bar{\chi}$  [20]. Here we have two kinds of signals consisting of the high energy neutrino and the boosted anti-dark matter whose energies are fixed at  $E_\nu = 3m_\chi/4$  and  $E_{\bar{\chi}} = 5m_\chi/4$  by the kinematics assuming non-relativistic initial states. Therefore these particles can be distinctive signals of the semi-annihilation process. Although we mainly focus on the case that the scattering cross section with a nucleon is proportional to the momentum transfer  $Q^{2n}$  ( $n = 1, 2$ ), we also consider a constant cross section ( $n = 0$ ) for comparison. Then we estimate the number of events for these neutrino/boosted dark matter signals from the Sun, and atmospheric neutrino backgrounds assuming the DUNE detector because it has advantage for the angular resolution compared to the other experiments. In addition, note that exploring the boosted dark matter with a mild boost factor as our case is difficult at Super-Kamiokande/Hyper-Kamiokande and IceCube/DeepCore because the boost factor is below the Cherenkov threshold:  $\gamma_{\text{Cherenkov}} = 1.51$  (water) and 1.55 (ice), respectively [9]. For this purpose, we use the neutrino event generator **GENIE** in order to produce the neutrino scattering events with nuclei [25]. In this code, the boosted

dark matter can also be implemented by slightly modifying the source code. We investigate the sensitivity at the DUNE experiment assuming 40 kton liquid argon detector with 10 years period of time [26].

The paper is organized as follows. In Section 2, we describe the setup for our calculations, and estimate the number of signal events and atmospheric neutrino backgrounds. In Section 3, we illustrate how to reconstruct the signal events, and indicate the kinematic cuts, the energy/momentum thresholds and resolutions of the DUNE detector. Section 4 is devoted to present the numerical results and interpretations. We summarize our work in Section 5.

## 2 Setup

We consider the dark matter semi-annihilation  $\chi\chi \rightarrow \nu\bar{\chi}$  where the dark matter  $\chi$  must be a Dirac fermion to allow this process from the spin conservation [20]. In general, the CP conjugate process  $\bar{\chi}\bar{\chi} \rightarrow \bar{\nu}\chi$  is also allowed. However we concentrate only on  $\chi\chi \rightarrow \nu\bar{\chi}$  to avoid unnecessary complication. This implies that the dark matter is asymmetric though it is not a requirement for the following discussion. Hereafter the anti-dark matter in the final state is simply regarded as dark matter because this simplification does not lead any substantial difference.<sup>1</sup> We assume that the dark matter abundance is thermally determined by the semi-annihilation, and forms the dark matter halo. Namely the magnitude of the cross section is fixed as  $\langle\sigma_{\text{semi}}v_{\text{rel}}\rangle \sim 10^{-26} \text{ cm}^3/\text{s}$ .

The dark matter particles are accumulated at the centre of the Sun due to the gravitational force. Then, the semi-annihilation  $\chi\chi \rightarrow \nu\bar{\chi}$  and the capture process  $\chi N \rightarrow \chi N$  easily equilibrate if the dark matter mass is  $m_\chi \gtrsim 4 \text{ GeV}$  [27] where  $N$  is nucleons. Therefore we can anticipate the simultaneous signals of the high energy neutrino and boosted dark matter from the Sun. Because the dark matter particles accumulated in the Sun are non-relativistic, the energies of the neutrino and boosted dark matter are kinematically fixed to be  $E_\nu = 3m_\chi/4$  and  $E_\chi = 5m_\chi/4$ , and the corresponding speed of the boosted dark matter is  $v_\chi = 0.6$ . We will explore these two kinds of signals at the DUNE experiment with 40 kton liquid argon fiducial volume and 10 years exposure [24]. The DUNE experiment may not be able to detect the particles with the energy larger than  $\mathcal{O}(100) \text{ GeV}$  due to the detector design [26]. Therefore we concentrate on the dark matter mass range:  $4 \text{ GeV} \leq m_\chi \leq 100 \text{ GeV}$  in this work.

The concrete ultra-violet complete models leading the semi-annihilation process  $\chi\chi \rightarrow \nu\bar{\chi}$  have been studied in refs. [28, 29] for example. In addition, similar discussions can be done for another semi-annihilation process  $\chi\chi \rightarrow J\bar{\chi}$  in a concrete model [30] where  $J$  is a Majoron being the Nambu-Goldstone boson associated with the global lepton number

---

<sup>1</sup>A difference may arise for neutrinos because the neutrino interactions are different from the anti-neutrino ones.

symmetry. The produced Majoron subsequently decays into neutrinos  $J \rightarrow \nu\nu$ . Model building is out of scope in this work, and we concentrate on the calculation of the signal events with the parametrization of the cross section as will be given in Eq. (2.7) later.

## 2.1 Neutrino signal and background

The neutrino flux produced by the dark matter semi-annihilation  $\chi\chi \rightarrow \nu\bar{\chi}$  coming from the Sun, is given by

$$\frac{d^2\Phi_\nu}{dE_\nu d\Omega} = \frac{\Gamma_{\text{ann}}}{4\pi d_\odot^2} \delta\left(E_\nu - \frac{3}{4}m_\chi\right) \delta(\Omega - \Omega_\odot), \quad (2.1)$$

where  $d_\odot = 1.50 \times 10^{13}$  cm is the distance between Earth and the Sun,  $\Omega_\odot$  is the Sun's solid angle, and  $\Gamma_{\text{ann}}$  is the semi-annihilation rate which is simply related with the capture rate in the Sun  $C_\odot$  as  $\Gamma_{\text{ann}} = C_\odot/2$  under the assumption that the dark matter capture and semi-annihilation processes equilibrate in the Sun [31]. For the case that the cross section for  $\chi N \rightarrow \chi N$  is a constant or is proportional to the momentum transfer  $Q^2$ , the capture rate is shown in Fig. 1 where  $\sigma_{\chi N} = 10^{-40}$  cm<sup>2</sup> is assumed for the dark matter velocity  $v_\chi \sim 10^{-3}$ , and the capture rate simply scales as  $C_\odot \propto \sigma_{\chi N}$  [27]. One can easily understand that the  $Q^2$  dependent capture rate is larger than the constant case because the dark matter velocity is accelerated by the Sun's gravitational force when the dark matter is captured. As we will see later, we also consider the  $Q^4$  dependent case. The  $Q^4$  dependent capture rate is simply obtained by scaling the  $Q^2$  dependent one with the factor 590 for the spin-independent (SI) and 50 for spin-dependent (SD) cross sections. This is based on the simple extrapolation of the relation between the constant and the  $Q^2$  dependent capture rates as can be seen in Fig. 1.

The high energy neutrino produced by the semi-annihilation  $\chi\chi \rightarrow \nu\bar{\chi}$  enters in the DUNE detector and scatters off the nucleons in argon nuclei via the charged-current (CC) interaction. As a result, a charged lepton and some number of nucleons (a jet) are generated due to hadronization. Thus a pair of a charged lepton and a jet can be regarded as the signal event for the neutrino. The number of the neutrino signal events is calculated as

$$N_\nu^{\text{CC}} = N_N T \sum_\alpha \int \sigma_{\nu_\alpha N}^{\text{CC}} \frac{d^2\Phi_{\nu_\alpha}}{dE_{\nu_\alpha} d\Omega} dE_{\nu_\alpha} d\Omega, \quad (2.2)$$

where  $\alpha$  is the neutrino flavor index ( $e, \bar{e}, \mu, \bar{\mu}$ ), the neutrino flux  $d^2\Phi_{\nu_\alpha}/dE_{\nu_\alpha} d\Omega$  is given by Eq. (2.1),  $N_N = 2.41 \times 10^{34}$  is the number of nucleons in liquid argon target (assuming 40 kton fiducial volume),  $T = 10$  yr is the period of the experiment, and  $\sigma_{\nu_\alpha N}^{\text{CC}}$  is the neutrino-nucleon scattering cross section for argon via the CC interaction. Integrating

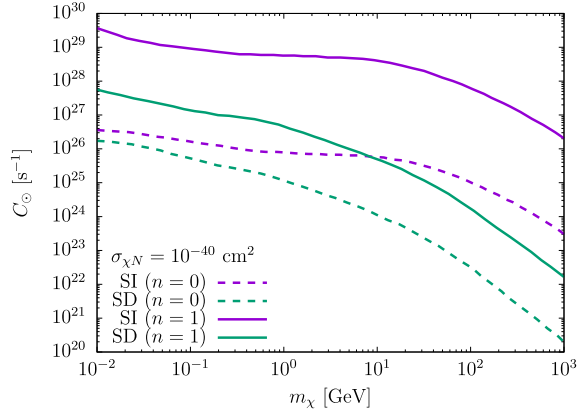


Figure 1: Dark matter capture rate in the Sun with  $\sigma_{\chi N} = 10^{-40} \text{ cm}^2$  [27]. The solid purple line represents for spin-independent (SI) cross sections with  $Q^2$  dependence ( $n = 1$ ) while the solid green line is for spin-dependent (SD) cross sections. The dashed purple and green lines are for constant cross sections ( $n = 0$ ). The index  $n = 0, 1$  labels the dependence of the momentum transfer  $Q^2$  (See Eq. (2.7)).

over the energy and the solid angle, we obtain

$$N_{\nu}^{\text{CC}} = N_N T \sum_{\alpha} \frac{C_{\odot}}{8\pi d_{\odot}^2} \sigma_{\nu_{\alpha} N}^{\text{CC}} \Big|_{E_{\nu_{\alpha}}=3m_{\chi}/4}. \quad (2.3)$$

Precise evaluation of the cross section is difficult especially around  $E_{\nu} = \mathcal{O}(1)$  GeV because of the complicated nuclear interactions. Here we adopt the evaluation based on the experimental nuclear model implemented in GENIE. The extracted CC (and neutral-current (NC)) cross sections in argon target are shown in Fig. 2. One can easily confirm that these CC cross sections are consistent with the various experimental measurements [33].

The main background for the neutrino signal is atmospheric neutrinos ( $\nu_{\text{atm}} + N \rightarrow \ell + j$ ) whose number of events for each flavor is calculated as

$$N_{\text{atm } \nu_{\alpha}}^{\text{CC}} = N_N T \int \sigma_{\nu_{\alpha} N}^{\text{CC}} \frac{d^2 \Phi_{\nu_{\alpha}}^{\text{atm}}}{dE_{\nu_{\alpha}} d\Omega} dE_{\nu_{\alpha}} d\Omega, \quad (2.4)$$

where  $d^2 \Phi_{\nu_{\alpha}}^{\text{atm}} / dE_{\nu_{\alpha}} d\Omega$  is the atmospheric neutrino flux for the neutrino flavor  $\alpha$ . We use the atmospheric neutrino fluxes at Homestake based on HAKKM2014 model [34, 35], and average the fluxes with the minimum and maximum solar modulation effect. For the solid angle, we take into account the DUNE angular resolution ( $1^{\circ}$  for charged leptons and  $5^{\circ}$  for the others as will be seen in Tab. 1), and we obtain  $\Delta\Omega/4\pi = \pi \tan(1^{\circ} + 5^{\circ})/4\pi = 1.31 \times 10^{-2}$ . This is regarded as the effective solid angle for the DUNE detector because the actual Sun's solid angle is much smaller than that for the angular resolution. Thus

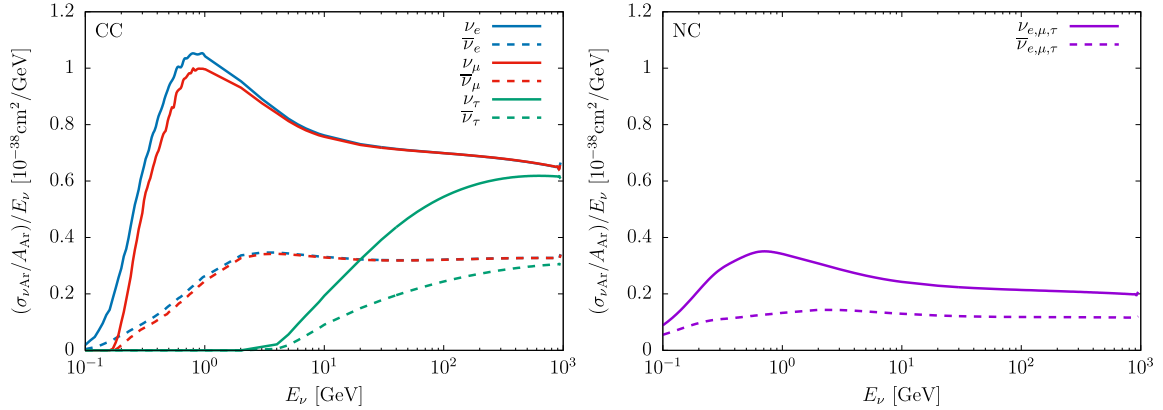


Figure 2: Neutrino-nucleon scattering cross sections in argon nuclei for CC (left) and NC (right) interactions [32] where  $A_{\text{Ar}} = 39.9$  is the argon mass number.

the number of events for the atmospheric neutrino background coming from the Sun is numerically evaluated as

$$N_{\text{atm } \nu_\alpha}^{\text{CC}} = N_N T \frac{\Delta\Omega}{4\pi} \int \sigma_{\nu_\alpha N}^{\text{CC}} \frac{d\Phi_{\nu_\alpha}^{\text{atm}}}{dE_{\nu_\alpha}} dE_{\nu_\alpha}. \quad (2.5)$$

Integrating over the atmospheric neutrino energy, the expected number of the atmospheric neutrino background for each flavor is estimated as

$$N_{\text{atm } \nu_e}^{\text{CC}} = 150.9, \quad N_{\text{atm } \nu_\mu}^{\text{CC}} = 29.47, \quad N_{\text{atm } \bar{\nu}_e}^{\text{CC}} = 265.6, \quad N_{\text{atm } \bar{\nu}_\mu}^{\text{CC}} = 64.26, \quad (2.6)$$

for 40 kton liquid argon and 10 years exposure, and the total number of events is 510.3. We take into account only electron and muon flavors of neutrinos, and tau flavor is not considered here. Regarding tau neutrino background, there is an argument in Ref. [19].

## 2.2 Boosted dark matter signal and background

For the scattering between the dark matter and nuclei, there are three kinds of relevant processes which are (quasi-)elastic, resonant and deep inelastic scattering (DIS) processes [19, 36]. The dominant process changes depending on the magnitude of the momentum transfer  $Q^2$  which is related with the Mandelstam variable as  $t = -Q^2$ . For the semi-annihilation process  $\chi\chi \rightarrow \nu\bar{\chi}$  we focus on, the dark matter velocity is fixed at  $v_\chi = 0.6$  by kinematics and the range of the momentum transfer is approximately limited in  $Q^2 \lesssim 9m_N^2/4 \approx (1.4 \text{ GeV})^2$  for  $m_N \ll m_\chi$ . In this energy range, the (quasi-)elastic scattering is dominant over the other processes.

We parametrize the differential elastic scattering cross section for  $\chi N \rightarrow \chi N$  as [27]

$$\frac{d\sigma_{\chi N}}{dQ^2} = \frac{\sigma_0 s}{4m_N^2 |\mathbf{p}_\chi|^2} \left( \frac{Q^2}{m_N^2 v_0^2} \right)^n |F(Q^2)|^2, \quad (2.7)$$

where  $s$  is the Mandelstam variable,  $|\mathbf{p}_\chi| = 3m_\chi/4$  is the initial dark matter momentum,  $v_0 = 220$  km/s is a reference speed of dark matter, and  $\sigma_0$  is a reference cross section. The index  $n$  represents the order of momentum transfer dependence and we take  $n = 0, 1, 2$ . For the form factor  $F(Q^2)$ , we adopt a dipole form factor described by [19]

$$F(Q^2) = \frac{F(0)}{(1 + Q^2/M^2)^2}, \quad (2.8)$$

where the normalization factor can be regarded as  $F(0) = 1$  because it is absorbed by the reference cross section  $\sigma_0$ , and the reference mass is  $M = 0.99$  GeV.<sup>2</sup> The total scattering cross section can be obtained by integrating in the range  $0 < Q^2 < \lambda(s, m_\chi^2, m_N^2)/s$  where  $\lambda(x, y, z) = x^2 + y^2 + z^2 - 2xy - 2yz - 2xz$  is the kinematic function (Källén function). Note that the differential cross section in Eq. (2.7) is related to the non-relativistic elastic cross section  $\sigma_{\chi N}^0$  relevant to dark matter direct detection as

$$\sigma_{\chi N}^0 = \frac{\sigma_0}{n+1} \left( \frac{2m_\chi}{m_\chi + m_N} \right)^{2n}, \quad (2.9)$$

which is obtained by integrating over  $Q^2$  with  $F(Q^2) = 1$  and  $|\mathbf{p}_\chi| = m_\chi v_0$ .

Similar to the neutrino signal in the previous subsection, the number of the boosted dark matter signal events is calculated as

$$N_\chi = N_N T \int \sigma_{\chi N} \frac{d^2\Phi_\chi}{dE_\chi d\Omega} dE_\chi d\Omega, \quad (2.10)$$

where  $d^2\Phi_\chi/dE_\chi d\Omega$  is the boosted dark matter flux produced by the dark matter semi-annihilation  $\chi\chi \rightarrow \nu\bar{\chi}$ , which can be given by

$$\frac{d^2\Phi_\chi}{dE_\chi d\Omega} = \frac{\Gamma_{\text{ann}}}{4\pi d_\odot^2} \delta\left(E_\chi - \frac{5}{4}m_\chi\right) \delta(\Omega - \Omega_\odot). \quad (2.11)$$

Integrating over the energy and the solid angle, we obtain

$$N_\chi = N_N T \frac{C_\odot}{8\pi d_\odot^2} \sigma_{\chi N} \Big|_{E_\chi=5m_\chi/4}. \quad (2.12)$$

The main background for the boosted dark matter signal is atmospheric neutrinos via the NC interaction ( $\nu_{\text{atm}} + N \rightarrow \nu_{\text{atm}} + N$ ). The number of events for the background is calculated as

$$N_{\text{atm}\nu_\alpha}^{\text{NC}} = N_N T \int \sigma_{\nu_\alpha N}^{\text{NC}} \frac{d^2\Phi_{\nu_\alpha}^{\text{atm}}}{dE_{\nu_\alpha} d\Omega} dE_{\nu_\alpha} d\Omega, \quad (2.13)$$

where  $\sigma_{\nu_\alpha N}^{\text{NC}}$  is the neutrino–nucleon cross section in argon nuclei via the NC interaction, which is extracted from GENIE and shown in the right panel of Fig. 2. Integrating over

---

<sup>2</sup>In fact, the shape of the form factor depends on unknown dark matter interactions.

the atmospheric neutrino energy, the expected number of the background for each flavor is estimated as

$$N_{\text{atm}\nu_e}^{\text{NC}} = 59.30, \quad N_{\text{atm}\nu_\mu}^{\text{NC}} = 20.38, \quad N_{\text{atm}\bar{\nu}_e}^{\text{NC}} = 117.8, \quad N_{\text{atm}\bar{\nu}_\mu}^{\text{NC}} = 47.67, \quad (2.14)$$

for 40 kton liquid argon and 10 years exposure, and the total number of events is 245.2.

The monochromatic neutrino signals with  $E_\nu = 3m_\chi/4$  discussed in the previous subsection may also be a background for the boosted dark matter signal. However, the dominant process is the DIS for this case because the neutrino energy is much larger than  $\mathcal{O}(1)$  GeV, and we can easily discard these events from the background.

From the above argument, one can see that the number of events for the boosted dark matter is roughly proportional to the square of the elastic scattering cross section between dark matter and nucleons as in Eq. (2.12) (the capture rate is also proportional to  $\sigma_{\chi N}$ ). On the other hand, the number of events for the neutrino signal is simply proportional to the elastic scattering cross section coming from the capture rate as can be seen Eq. (2.3).

### 3 Event reconstruction

We generate the neutrino and boosted dark matter signals using `GENIE` [25], and assume those signals are detected at the DUNE detector. The detector threshold, energy/momentum resolution and angular resolution are shown in Tab. 1. In particular, DUNE has good angular resolution for charged leptons and gamma. We apply it for the signal event search below. Namely, the events below the threshold will be discarded, and the generated observables such as a momentum/energy and angle will be smeared with the energy/momentum and angular resolutions. Then we regard the event is observed only if the reconstructed energy after smearing is within the  $2\sigma$  energy resolution. In the following, we show how to reconstruct the signals from the observed quantities.

If one would like to take into account the seasonal modulation of the signal events from the Sun, the public code `GenSolFlux` [36] and `SolTrack` [37] can be used though we do not consider in our work.

#### 3.1 Neutrino energy reconstruction

The high energy neutrinos produced by the dark matter semi-annihilation generate a charged lepton and a jet via the CC interaction at the DUNE detector as illustrated in the left panel of Fig. 3 where the jet is constructed by several number of nucleons, charged pions and gamma. The energy of the charged lepton ( $E_\ell$ ) and the direction of the charged lepton ( $\theta_\ell$ ) and jet ( $\theta_j$ ) can be identified with high precision at DUNE while the jet energy is not so precise. Using these observed quantities, one can reconstruct the

	Detector threshold	Energy/momentum resolution	Angular resolution
$\mu^\pm$	30 MeV	5 %	1°
$\pi^\pm$	100 MeV	5 %	1°
$e^\pm/\gamma$	30 MeV	$2 + 15/\sqrt{E/\text{GeV}}$ %	1°
$p$	50 MeV	$ \mathbf{p}  < 400$ MeV: 10 % $ \mathbf{p}  > 400$ MeV: $5 + 30/\sqrt{E/\text{GeV}}$ %	5°
$n$	50 MeV	$40/\sqrt{E/\text{GeV}}$ %	5°

Table 1: Detector threshold, energy/momentum resolution and angular resolution of the DUNE detector [26].

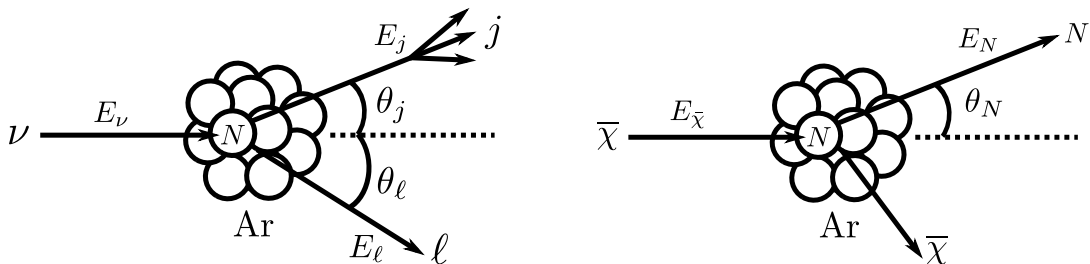


Figure 3: (Left): momenta and angles of the charged lepton  $\ell$  and jet  $j$  in the final state. These quantities can be identified with good precision at DUNE. (Right): kinematics for the elastic scattering of the boosted dark matter signal.

neutrino energy as [38]

$$E_\nu = \frac{1}{2} \frac{\sin \theta_j (1 + \cos \theta_\ell) + \sin \theta_\ell (1 + \cos \theta_j)}{\sin \theta_j} E_\ell. \quad (3.1)$$

The angles  $\theta_\ell$  and  $\theta_j$  are expected to be very small for the neutrino energy  $E_\nu \gtrsim \mathcal{O}(1)$  GeV.

### 3.2 Boosted dark matter energy reconstruction

For the boosted dark matter, the scattering kinematics is simply determined because the main process is quasi-elastic scattering  $\chi N \rightarrow \chi N$  in our case. We define the recoil nucleon energy  $E_N$  and the angle  $\theta_N$  measured from the solar direction as shown in the right panel of Fig. 3. Thus using the energy/momentum conservation, the boosted dark matter energy  $E_\chi$  can be reconstructed as

$$E_\chi = m_N \frac{1 + \alpha \cos \theta_N \sqrt{1 - \beta + \alpha^2 \beta \cos^2 \theta_N}}{-1 + \alpha^2 \cos^2 \theta_N}, \quad (3.2)$$

where  $\alpha = \sqrt{(E_N + m_N)/(E_N - m_N)} > 1$  and  $\beta = m_\chi^2/m_N^2 > 1$ . Therefore the incoming boosted dark matter energy can be reconstructed from the observables  $E_N$  and  $\theta_N$ . Be-

	model	$m_\chi$ [GeV]	$\sigma_0$ [cm <sup>2</sup> ]	# of $\nu$ events	# of $\chi$ events
BP1	SD ( $n = 1$ )	10	$3.0 \times 10^{-43}$	$N_{\text{atm } \nu}^{\text{CC}} = 510/510$ $N_\nu^{\text{CC}} = 56/56$	$N_{\text{atm } \nu}^{\text{NC}} = 35/245$ $N_\chi = 14/40$
BP2	SI ( $n = 2$ )	20	$7.0 \times 10^{-50}$	$N_{\text{atm } \nu}^{\text{CC}} = 510/510$ $N_\nu^{\text{CC}} = 20/20$	$N_{\text{atm } \nu}^{\text{NC}} = 46/245$ $N_\chi = 774/2396$

Table 2: Benchmark parameter sets and the observed/expected number of events after the cut with the detector threshold and resolution. For the number of events, the neutrino flavors ( $\alpha = e, \bar{e}, \mu, \bar{\mu}$ ) are summed.

cause the velocity of the boosted dark matter is moderate ( $v_\chi = 0.6$ ), the scattering angle  $\theta_N$  is widely spread unlike the above neutrino case.

For the quasi-elastic scattering, several number of nucleons may be produced in the final state due to hadronization. We take the events with only one nucleon in the final state because the resolution uncertainty becomes larger if several number of nucleons are produced. Although this choice lowers the detector efficiency as we will see later, the precision of the energy reconstruction is much higher. We have numerically checked that approximately 32% of the quasi-elastic scattering events involve only one nucleon.

## 4 Results

### 4.1 Benchmark parameter sets

Two benchmark parameter sets and the observed/expected number of events after the cut with the detector threshold and resolution are shown in Tab. 2. The BP1 has relatively the small number of boosted dark matter signal events  $N_\chi$  while the BP2 has a large number. This is because the  $n = 2$  model has a strong dependence of the momentum transfer  $Q^2$ . Fig. 4 shows the reconstructed energy distributions of the neutrino and boosted dark matter for BP1 (upper panels) and BP2 (lower panels). The blue, red and black lines correspond to the number of the atmospheric neutrino background, the neutrinos/boosted dark matter signals and sum of those events, respectively. The most of the reconstructed energy of the atmospheric neutrino background has a few GeV as expected from the energy flux. The actual energies are  $E_\nu = 7.5$  GeV and  $E_\chi = 12.5$  GeV for the BP1 while those are  $E_\nu = 15$  GeV and  $E_\chi = 25$  GeV for the BP2. One can find from the plots that the energies of the neutrino and boosted dark matter signals are reconstructed well with a dispersion.

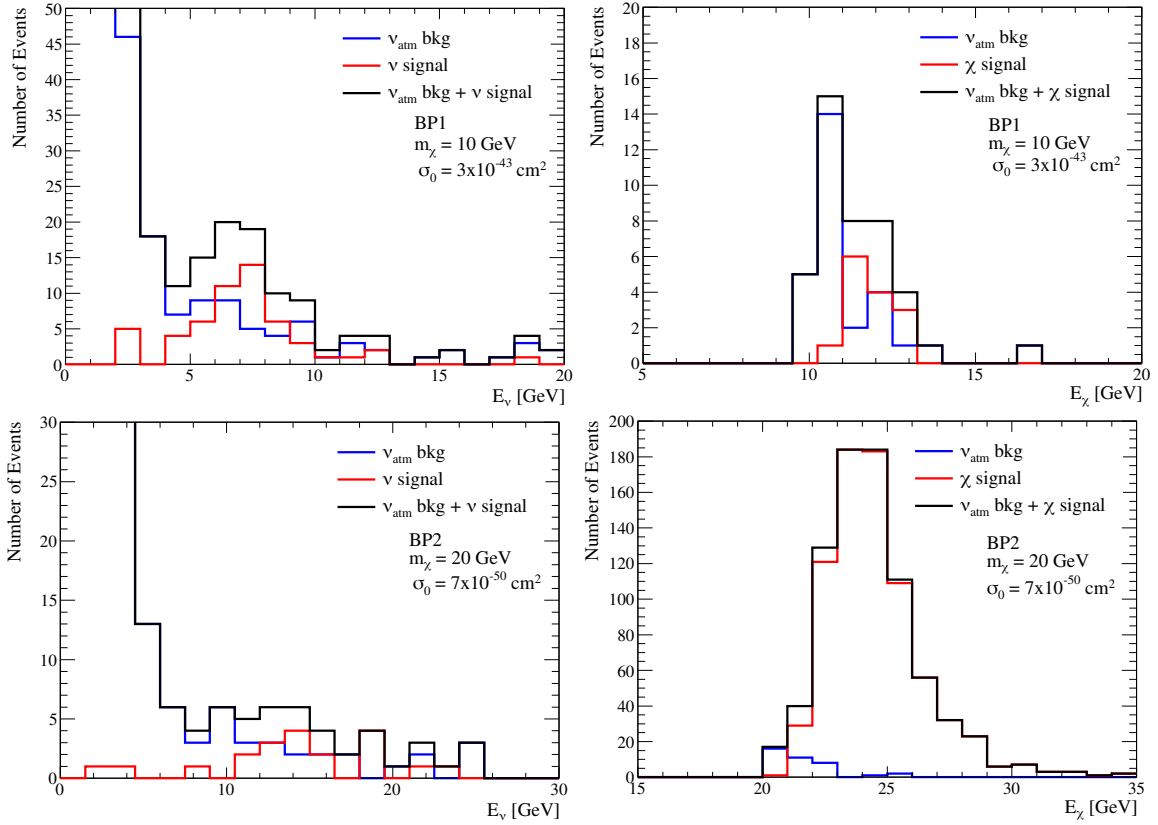


Figure 4: Reconstructed neutrino energy distribution (left) and boosted dark matter energy distribution (right). The upper (lower) panel corresponds to BP1 (BP2) in Tab. 2. The red, blue and black lines represent the number of events for atmospheric neutrino background, neutrino/boosted dark matter signal and sum of them, respectively.

## 4.2 Parameter space

We search for the parameter space testable by DUNE in  $(m_\chi, \sigma_0)$  plane. For this purpose, we define the signal significance with

$$\mathcal{S}_\nu = \frac{N_\nu^{\text{CC}}}{\sqrt{N_{\text{atm}\nu}^{\text{CC}} + N_\nu^{\text{CC}}}}, \quad (4.1)$$

$$\mathcal{S}_\chi = \frac{N_\chi}{\sqrt{N_{\text{atm}\nu}^{\text{NC}} + N_\chi}}, \quad (4.2)$$

for the neutrino and boosted dark matter signals, respectively. For the constant cross section ( $n = 0$ ), the  $2\sigma$  DUNE sensitivity is shown in Fig. 5 for the SI (left) and SD (right) cross sections. The solid blue and red lines represent the DUNE sensitivities for the neutrino and boosted dark matter signals. Namely, the above region from each line can be searched by DUNE. The black and orange regions are excluded by the direct detection experiments (LZ [3], XENON1T [1] and PICO 60 [39]). The dashed black

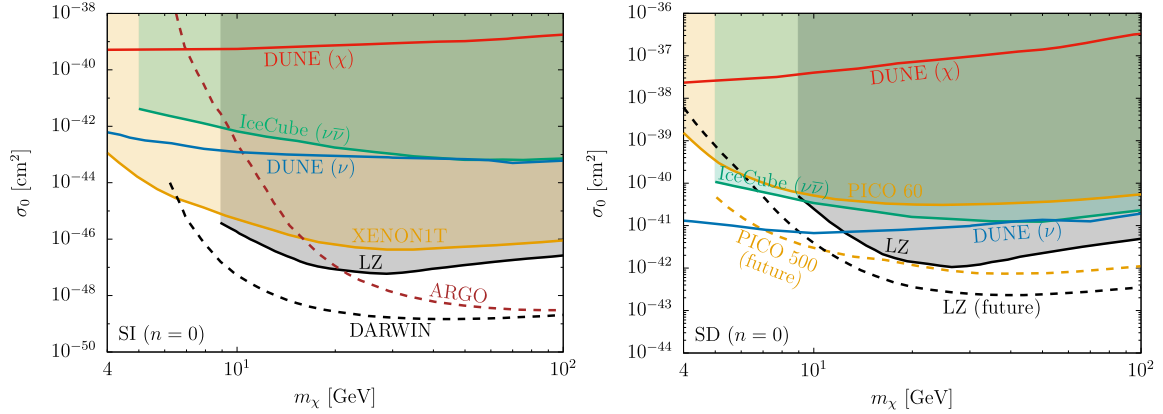


Figure 5: DUNE sensitivity at  $2\sigma$  for the neutrino (blue) and boosted dark matter (red) signals ( $n = 0$ ). The existing upper bounds and future sensitivities for dark matter cross section  $\sigma_0$  are also shown. The black and orange regions are excluded by the direct detection experiments (LZ [3], XENON1T [1] and PICO 60 [39]) while the green region is excluded by the monochromatic neutrino observation at IceCube [45]. The dashed black and brown lines on the left panel are the future sensitivities of DARWIN [40, 41] and ARGO [42] while the dashed black and orange lines on the right panel are the future sensitivities of LZ [43] and PICO 500 [44].

(DARWIN [40, 41]) and brown (ARGO [42]) lines on the left upper panel represent the future sensitivities of direct detection experiments for the SI case while the dashed black (LZ [43]) and orange (PICO 500 [44]) lines on the right upper panel correspond to the SD case. The green region on the right upper panel is excluded by the monochromatic neutrino observation at IceCube [45]. The green region for the left upper panel has been obtained by translating the original IceCube bound for the SD cross section into the SI cross section with the corresponding capture rates. Because the constraint of the direct detection experiments is very strong, all the parameter space for the boosted dark matter which can be tested by DUNE (the upper region from the red line) is completely excluded as expected.

Fig. 6 shows the parameter space for the  $n = 1$  and  $n = 2$  cases. There is no substantial bound from the direct detection experiments for these cases because the non-relativistic elastic cross section is highly suppressed by a small momentum transfer. However the IceCube bound still exists as indirect detection because the high energy neutrino always accompanied by the boosted dark matter in our setup. The IceCube bounds for the  $n = 1$  and  $n = 2$  cases have been obtained as same as the left panel in Fig. 5 by translating the IceCube bound for the SD ( $n = 0$ ) cross section [45]. The black stars represent the benchmark parameter sets (BP1 and BP2) discussed in the previous section.

For  $n = 2$ , the DUNE sensitivity for the boosted dark matter becomes much higher

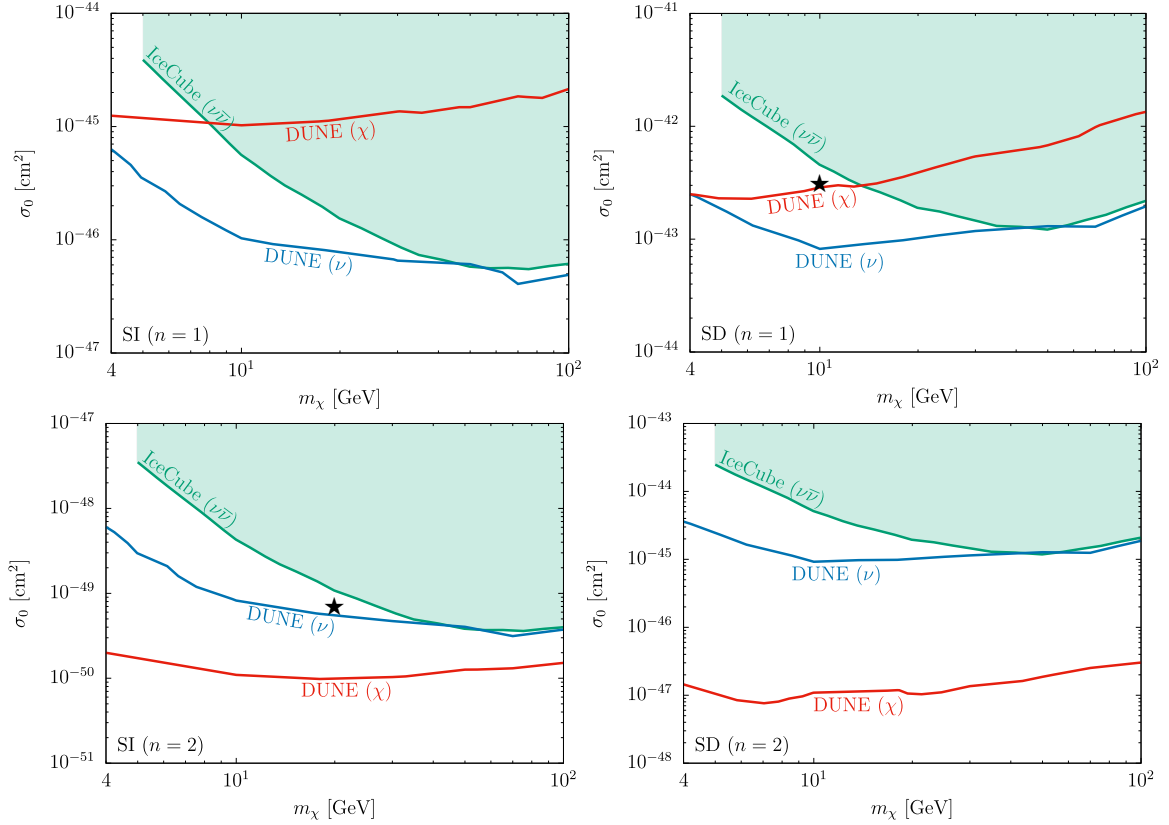


Figure 6: Same plots with Fig. 5 for  $n = 1$  and 2. The black stars represent the benchmark parameter sets (BP1 and BP2).

than the other cases. This is expected because the capture rate in the Sun becomes larger for  $n = 2$  due to the gravitational force when the dark matter is captured, and there is no strong bound from the direct detection experiments. In addition, it can be seen that the dark matter mass range that the DUNE experiment can test is approximately below 30 GeV due to the IceCube bound.

We comment on a lighter dark matter case ( $m_\chi \lesssim 4$  GeV). In this case, the elastic scattering and dark matter semi-annihilation processes may not equilibrate. Therefore an extra suppression factor would be multiplied to the capture rate in Eqs. (2.3) and (2.12), and the DUNE sensitivity is anticipated to be weaker than the naive extrapolation of the DUNE sensitivity lines in Fig. 5.

## 5 Summary

No dark matter signal at direct detection experiments may infer that the elastic scattering cross section between dark matter and nucleons is suppressed by a small momentum transfer. Such kind of dark matter can be explored by the large neutrino volume detectors

if the dark matter is boosted by some mechanism. In this work, we considered the dark matter semi-annihilation process  $\chi\chi \rightarrow \nu\bar{\chi}$ , which produce the high energy neutrino and boosted dark matter simultaneously. These produced particles can be a distinctive signal of the dark matter semi-annihilation. In particular, dark matter particles are accumulated in the centre of the Sun, and the semi-annihilation produces the monochromatic neutrino and boosted dark matter. We parametrized the differential cross section between dark matter and nucleons for three different cases as in Eq. (2.7) with  $n = 0, 1$  and  $2$ . Then we generated the signal events and atmospheric neutrino background events using **GENIE**, and estimated the detection sensitivity at DUNE. We found that the simultaneous detection of the neutrino and boosted dark matter at DUNE is possible in some parameter space for  $n = 1$  and  $2$  (momentum transfer dependent cases) while  $n = 0$  (constant case) is completely ruled out by the current direct detection experiments as one can easily expect. We found that the dark matter mass region which is testable at DUNE is below 30 GeV.

## Acknowledgments

The authors would like to thank the members of the GENIE working group, especially Costas Andreopoulos, Joshua Barrow, Joshua Berger and Robert Hatcher for helping to use **GENIE**. This work was supported by JSPS KAKENHI Grant Numbers 20H00160, 23K03384 and 23H04004.

## References

- [1] E. Aprile *et al.* [XENON], Phys. Rev. Lett. **121**, no.11, 111302 (2018) [[arXiv:1805.12562](#) [astro-ph.CO]].
- [2] Y. Meng *et al.* [PandaX-4T], Phys. Rev. Lett. **127**, no.26, 261802 (2021) [[arXiv:2107.13438](#) [hep-ex]].
- [3] J. Aalbers *et al.* [LZ], [[arXiv:2207.03764](#) [hep-ex]].
- [4] C. Gross, O. Lebedev and T. Toma, Phys. Rev. Lett. **119**, no.19, 191801 (2017) [[arXiv:1708.02253](#) [hep-ph]].
- [5] S. Ipek, D. McKeen and A. E. Nelson, Phys. Rev. D **90**, no.5, 055021 (2014) [[arXiv:1404.3716](#) [hep-ph]].
- [6] J. M. Cline, M. Puel and T. Toma, [[arXiv:2308.01333](#) [hep-ph]].
- [7] M. Aoki, M. Duerr, J. Kubo and H. Takano, Phys. Rev. D **86**, 076015 (2012) [[arXiv:1207.3318](#) [hep-ph]].
- [8] M. Aoki, J. Kubo and H. Takano, Phys. Rev. D **87**, no.11, 116001 (2013) [[arXiv:1302.3936](#) [hep-ph]].

- [9] K. Agashe, Y. Cui, L. Necib and J. Thaler, JCAP **10**, 062 (2014) [[arXiv:1405.7370](#) [hep-ph]].
- [10] M. Aoki, J. Kubo and H. Takano, Phys. Rev. D **90**, no.7, 076011 (2014) [[arXiv:1408.1853](#) [hep-ph]].
- [11] K. Kong, G. Mohlabeng and J. C. Park, Phys. Lett. B **743**, 256-266 (2015) [[arXiv:1411.6632](#) [hep-ph]].
- [12] J. Kopp, J. Liu and X. P. Wang, JHEP **04**, 105 (2015) [[arXiv:1503.02669](#) [hep-ph]].
- [13] H. Alhazmi, K. Kong, G. Mohlabeng and J. C. Park, JHEP **04**, 158 (2017) [[arXiv:1611.09866](#) [hep-ph]].
- [14] M. Aoki, D. Kaneko and J. Kubo, Front. in Phys. **5**, 53 (2017) [[arXiv:1711.03765](#) [hep-ph]].
- [15] M. Aoki and T. Toma, JCAP **10**, 020 (2018) [[arXiv:1806.09154](#) [hep-ph]].
- [16] D. Kim, J. C. Park and S. Shin, Phys. Rev. D **100**, no.3, 035033 (2019) [[arXiv:1903.05087](#) [hep-ph]].
- [17] J. Berger, Y. Cui and Y. Zhao, JCAP **02**, 005 (2015) [[arXiv:1410.2246](#) [hep-ph]].
- [18] K. J. Kelly and Y. Zhang, Phys. Rev. D **99**, no.5, 055034 (2019) [[arXiv:1901.01259](#) [hep-ph]].
- [19] J. Berger, Y. Cui, M. Graham, L. Necib, G. Petrillo, D. Stocks, Y. T. Tsai and Y. Zhao, Phys. Rev. D **103**, no.9, 095012 (2021) [[arXiv:1912.05558](#) [hep-ph]].
- [20] T. Toma, Phys. Rev. D **105**, no.4, 043007 (2022) [[arXiv:2109.05911](#) [hep-ph]].
- [21] M. G. Aartsen *et al.* [IceCube], Eur. Phys. J. C **75**, no.10, 492 (2015) [[arXiv:1505.07259](#) [astro-ph.HE]].
- [22] K. Choi *et al.* [Super-Kamiokande], Phys. Rev. Lett. **114**, no.14, 141301 (2015) [[arXiv:1503.04858](#) [hep-ex]].
- [23] K. Abe *et al.* [Hyper-Kamiokande], [[arXiv:1805.04163](#) [physics.ins-det]].
- [24] B. Abi *et al.* [DUNE], [[arXiv:2002.03005](#) [hep-ex]].
- [25] C. Andreopoulos, A. Bell, D. Bhattacharya, F. Cavanna, J. Dobson, S. Dytman, H. Gallagher, P. Guzowski, R. Hatcher and P. Kehayias, *et al.* Nucl. Instrum. Meth. A **614**, 87-104 (2010) [[arXiv:0905.2517](#) [hep-ph]].
- [26] R. Acciarri *et al.* [DUNE], [[arXiv:1512.06148](#) [physics.ins-det]].
- [27] R. Garani and S. Palomares-Ruiz, JCAP **05**, 007 (2017) [[arXiv:1702.02768](#) [hep-ph]].
- [28] E. Ma, Phys. Lett. B **662**, 49-52 (2008) [[arXiv:0708.3371](#) [hep-ph]].
- [29] M. Aoki and T. Toma, JCAP **09**, 016 (2014) [[arXiv:1405.5870](#) [hep-ph]].

- [30] T. Miyagi and T. Toma, JHEP **07**, 027 (2022) [[arXiv:2201.05412](#) [hep-ph]].
- [31] P. Baratella, M. Cirelli, A. Hektor, J. Pata, M. Piibeleht and A. Strumia, JCAP **03**, 053 (2014) [[arXiv:1312.6408](#) [hep-ph]].
- [32] C. Andreopoulos, C. Barry, S. Dytman, H. Gallagher, T. Golan, R. Hatcher, G. Perdue and J. Yarba, [[arXiv:1510.05494](#) [hep-ph]].
- [33] M. Tanabashi *et al.* [Particle Data Group], Phys. Rev. D **98**, no.3, 030001 (2018)
- [34] E. Richard *et al.* [Super-Kamiokande], Phys. Rev. D **94**, no.5, 052001 (2016) [[arXiv:1510.08127](#) [hep-ex]].
- [35] M. Honda, M. Sajjad Athar, T. Kajita, K. Kasahara and S. Midorikawa, Phys. Rev. D **92**, no.2, 023004 (2015) [[arXiv:1502.03916](#) [astro-ph.HE]].
- [36] J. Berger, [[arXiv:1812.05616](#) [hep-ph]].
- [37] M. van der Sluys, P. van Kan, and P. Sonneveld, AIP Conference Proceedings 1679 (2015), no. 1 080003, <https://aip.scitation.org/doi/10.1063/1.4931544>.
- [38] C. Rott, D. Jeong, J. Kumar and D. Yaylali, JCAP **07**, 006 (2019) [[arXiv:1903.04175](#) [astro-ph.HE]].
- [39] C. Amole *et al.* [PICO], Phys. Rev. D **100**, no.2, 022001 (2019) [[arXiv:1902.04031](#) [astro-ph.CO]].
- [40] M. Schumann, L. Baudis, L. Büttikofer, A. Kish and M. Selvi, JCAP **10**, 016 (2015) [[arXiv:1506.08309](#) [physics.ins-det]].
- [41] J. Aalbers *et al.* [DARWIN], JCAP **11**, 017 (2016) [[arXiv:1606.07001](#) [astro-ph.IM]].
- [42] GADMC Collaboration, C. Galbiati *et al.*, Future Dark Matter Searches with Low-Radioactivity Argon, Input to the European Particle Physics Strategy Update 2018-2020 (2018).
- [43] D. S. Akerib *et al.* [LZ], Phys. Rev. D **101**, no.5, 052002 (2020) [[arXiv:1802.06039](#) [astro-ph.IM]].
- [44] G. Giroux, J. Phys. Conf. Ser. **2156**, 012068 (2021)
- [45] R. Abbasi *et al.* [IceCube], Phys. Rev. D **105**, no.6, 062004 (2022) [[arXiv:2111.09970](#) [astro-ph.HE]].